TRACKING NONLINEAR EQUILIBRIUM PATHS BY A HOMOTOPY METHOD

by

Layne T. Watson
Siegfried M. Holzer
Mark C. Hansen

TECHNICAL REPORT NUMBER CS81001-R

TRACKING NONLINEAR EQUILIBRIUM PATHS BY A HOMOTOPY METHOD

Layne T. Watson[1]
Siegfried M. Holzer[2]
and
Mark C. Hansen[3]

Virginia Polytechnic Institute and State University,
Blacksburg, VA 24061, USA.

INTRODUCTION

In a comprehensive review of algorithms for numerical solution of nonlinear algebraic equations, Almroth and Felippa [1] state that "All standard forward integration schemes, whether corrected or not, exhibit inherent numerical instability near a critical point, a fact that limits the usefulness of those methods in postbuckling analysis." The homotopy method proposed here has no inherent numerical instability near a limit point, in fact, a limit point is no different (as far as the method is concerned) from any other point on the load-displacement curve. The method bears a superficial resemblance to standard continuation, imbedding, or incremental methods but is fundamentally different in two important respects: 1) Aside from bifurcation points, there are no "singular points" along the curve, so turning points (e.g., limit points) pose no special difficulties whatsoever; 2) the imbedding or load

---

[1]Associate Professor of Computer Science

[2]Professor of Civil Engineering

[3]Graduate Student

parameter λ is a dependent variable along the curve. In the algorithm, λ does not necessarily change monotonically, and part of the power of the algorithm derives from this ability of λ to both increase and decrease along the curve.

Theoretical background and results pertaining to the homotopy algorithm are in Refs. [2] and [3], and computer code is described in Refs. [4] and [5]. The method has been successfully applied to nonlinear complementarity problems [6], nonlinear two-point boundary value problems [3], fluid dynamics [7-9], highly nonlinear elastica problems [10], and optimal structural design [11].

HOMOTOPY METHOD

In the notation of Almroth and Felippa [1], the equilibrium equation has the form

$$F(q,\lambda,\bar{Q}) = 0 \tag{1}$$

where q is the generalized displacement vector, λ is the scalar load parameter, $\bar{Q}$ is the load distribution vector, and the vector function F is the force imbalance. q, $\bar{Q}$, and F are n-dimensional vectors, where n is the number of degrees of freedom. Note that F is viewed as a function of q, λ, and $\bar{Q}$. The theoretical basis for the homotopy algorithm is the following fact from differential geometry [2]:

FACT. Suppose that the $n \times (2n+1)$ Jacobian matrix of F

$$DF = [F_q \; F_\lambda \; F_{\bar{Q}}] \tag{2}$$

has full rank on $F^{-1}(0) = \{(q,\lambda,\bar{Q}) | F(q,\lambda,\bar{Q}) = 0, 0 \le \lambda < \infty\}$. Then for almost all $\bar{Q}$ the Jacobian matrix of

$$\tilde{F}(q,\lambda) = F(q,\lambda,\bar{Q}) \tag{3}$$

($\tilde{F}$ is just F with $\bar{Q}$ fixed) also has full rank on $\tilde{F}^{-1}(0) = \{(q,\lambda) | \tilde{F}(q,\lambda) = 0, 0 \le \lambda < \infty\}$.

"Almost all $\bar{Q}$" means for all $\bar{Q}$ except those in a set of measure zero. Alternatively, if $\bar{Q}$ were picked at random, the result holds with probability one. In practical terms, the conclusion is virtually always true. The full rank of the $n \times (n+1)$ Jacobian matrix

$$D\tilde{F} = \left[\tilde{F}_q \; \tilde{F}_\lambda\right] \tag{4}$$

at points on the load-displacement equilibrium curve Γ has two important consequences [2]: 1) Γ is a smooth curve with a continuously varying tangent, and Γ does not intersect itself nor other zero curves of $\tilde{F}$ (in the (n+1)-dimensional q, λ space). 2) the matrix $D\tilde{F}$ has a one dimensional kernel (null space), which is crucial to the implementation of the algorithm.

Since Γ is smooth, it may be parameterized by arc length s. Thus q and λ are functions of s along Γ, and eqn(1) becomes

$$\tilde{F}\big(q(s),\lambda(s)\big) = 0 \tag{5}$$

Thus

$$\frac{d}{ds}\tilde{F}\big(q(s),\lambda(s)\big) = \left[\tilde{F}_q\big(q(s),\lambda(s)\big) \; \tilde{F}_\lambda\big(q(s),\lambda(s)\big)\right]\begin{bmatrix}\frac{dq}{ds}\\ \frac{d\lambda}{ds}\end{bmatrix} = 0 \tag{6}$$

and

$$\left\| \begin{bmatrix} \frac{dq}{ds} \\ \frac{d\lambda}{ds} \end{bmatrix} \right\| = 1 \tag{7}$$

since Γ is parameterized by arc length - $q=q(s)$, $\lambda=\lambda(s)$ - and $\begin{bmatrix} \frac{dq}{ds}^T & \frac{d\lambda}{ds} \end{bmatrix}$ is the unit tangent vector to Γ pointing in the direction of increasing arc length. Γ is the trajectory of the initial value problem eqns(6) and (7) with initial conditions

$$q(0) = q_0, \quad \lambda(0) = 0 \tag{8}$$

zero

Tracking Γ simply amounts to solving eqns(6)-(8). Recall that the Jacobian matrix $\begin{bmatrix} \tilde{F}_q & \tilde{F}_\lambda \end{bmatrix}$ in eqn(6) has full rank everywhere along Γ, so in this formulation a limit point is oblivious. The true problem is to efficiently and accurately solve the initial value problem eqns(6)-(8) for $q(s)$, $\lambda(s)$.

Note that the derivative $\begin{bmatrix} \frac{dq}{ds}^T & \frac{d\lambda}{ds} \end{bmatrix}$ is only indirectly specified by eqns(6)-(7), and any ordinary differential equation algorithm requires the problem to be in the form

$$y' = f(s,y) \tag{9}$$

$\begin{bmatrix} \frac{dq}{ds}^T & \frac{d\lambda}{ds} \end{bmatrix}$ is calculated by finding the one-dimensional kernel of the matrix $\begin{bmatrix} \tilde{F}_q & \tilde{F}_\lambda \end{bmatrix}$ and then using eqn(7) and the continuity of the derivative. This kernel calculation is done via Householder reflections (see [2] for the details), and the work involved is comparable to solving a linear system of equations.

There are basically two approaches to tracking the curve Γ defined parametrically by $q=q(s)$, $\lambda=\lambda(s)$. The first is to use a low order ODE method (e.g., Euler's method) to predict the next point, and then use Newton's method with an $(n+1)\times(n+1)$ Jacobian matrix (formed by augmenting $\tilde{F}_q$ with a row and column to give a full rank matrix) to iterate back to Γ. This is simple, accurate (there is no drift from Γ), and has no difficulty with limit points. The disadvantages are that an appropriate step Δs for Euler's method is difficult to determine, there is no guarantee that the augmented matrix will have full rank, and iterating back to Γ exactly is very expensive if Euler's method is forced to take small steps to maintain convergence. See Rheinboldt [12] for an excellent discussion of and argument for this approach.

The second approach is to solve eqns(6)-(8) by a high order ODE method (e.g., a sophisticated variable step, variable order Adams method as in [13]), and use Newton's method only rarely to verify the accuracy of the ODE solver. Using an ODE subroutine package, this approach is simple, accurate enough for most engineering applications, and very efficient because Adams' methods are efficient. The step size selection and order choice are done automatically, relieving the user of two difficult and burdensome chores. Furthermore, a good implementation, as in [13], will be stable and robust. Drawbacks are that the solutions do

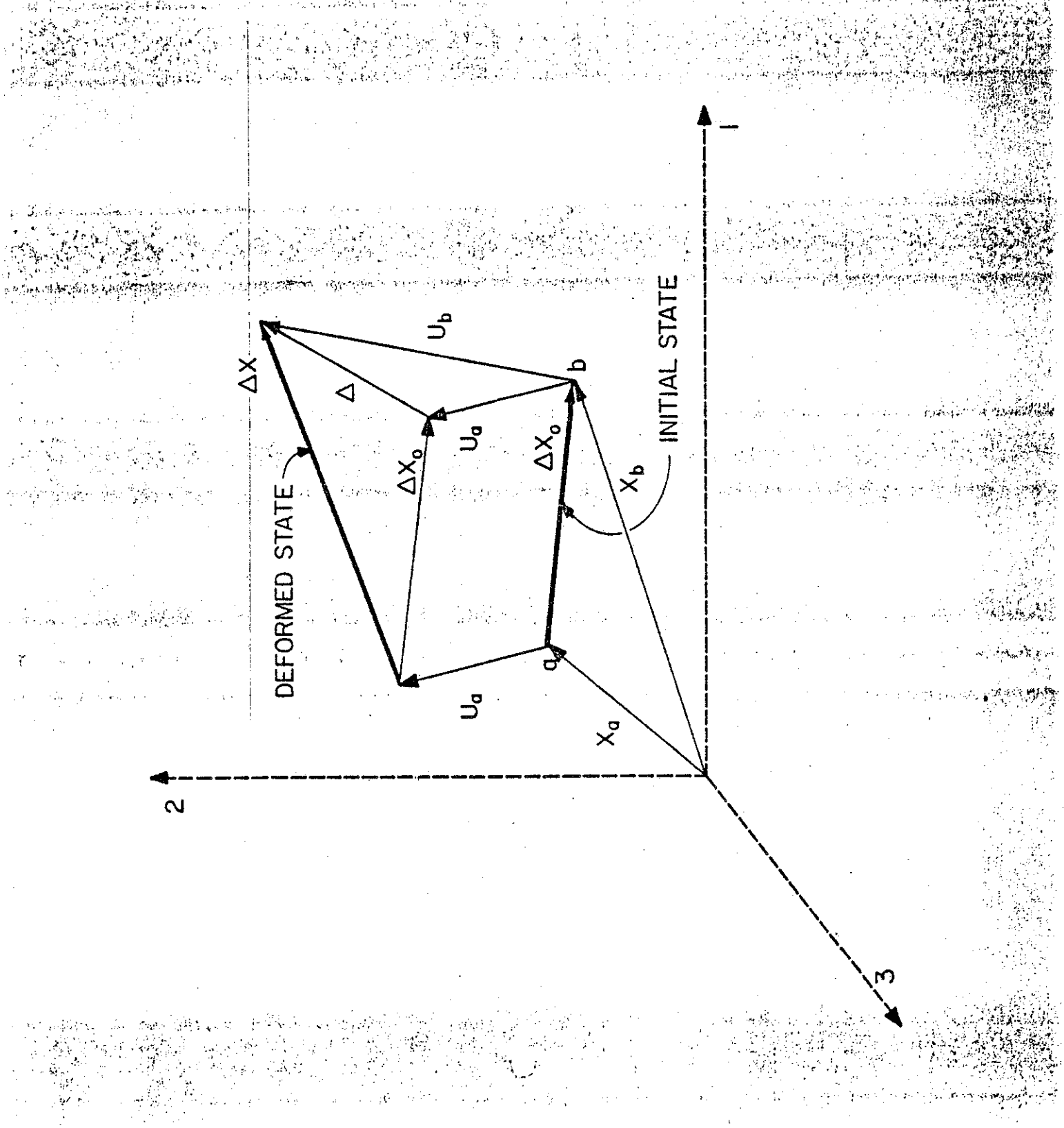
1
2
3
INITIAL STATE
DEFORMED STATE
ΔX
Δ
U_b
U_a
ΔX_o
ΔX_o
b
a
X_b
X_a
U_a

Fig. 1

drift (although slightly), the startup cost is high, and on rare occasions the method simply "loses" the curve and wanders off in the wrong direction.

Both approaches breeze through limit points with no difficulty, and neither approach is clearly superior. At the moment there is considerable computational evidence in favor of the second approach [2-11], and it is the second approach that is advocated here.

APPLICATION

The homotopy method was applied in the analysis of a space truss whose stability characteristics under multiple independent load combinations are described in Ref. [14]. A selection of results is presented. First, the mathematical model of space trusses, which is valid for large rotations [15], is expressed in the form of eqn 4.

MATHEMATICAL MODEL

The axial deformation of the truss element in Fig. 1 is

$$e = L - L_o \tag{10}$$

where L_o and L are the element lengths in the initial and deformed states, respectively. It follows from Fig. 1 that

$$L = ||\Delta X|| = \left(\sum_{j=1}^{3} L_j^2 \right)^{\frac{1}{2}} \tag{11}$$

$$L_o = ||\Delta X_o|| = \left(\sum_{j=1}^{3} L_{oj}^2\right)^{\frac{1}{2}} \tag{12}$$

$$L_j = L_{oj} + \Delta_j \tag{13}$$

$$\Delta X_o = X_b - X_a; \quad \Delta = U_b - U_a; \quad \Delta X = \Delta X_o + \Delta \tag{14}$$

where X_a, X_b are the initial coordinate vectors at the a, b-end of the element; U_a, U_b are the global displacement vectors at the a, b-end of the element; and the vectors ΔX_o, ΔX coincide with the initial, deformed state of the element. The strain energy of the element is

$$\Pi = \frac{1}{2} \gamma_o e^2; \quad \gamma = \frac{EA}{L_o} \tag{15}$$

where γ_o is the extensional stiffness of the element.

The principle of virtual work yields the equation of equilibrium

$$F(q, \lambda, \bar{Q}) = -\lambda \bar{Q} + \sum_{i=1}^{m} R^i = 0 \tag{16}$$

where

$$R_k^i = \frac{\partial \Pi^i}{\partial q_k}; \quad k = 1, 2, \ldots, n \tag{17}$$

The superscript i identifies the m elements of the assemblage. If Newton's method is used to verify the accuracy of the ODE solver, the generalized force vector of element i, R^i, is computed by the code number method [16] from the global force vector of element i, which can be expressed as

$$p^i = \begin{bmatrix} p_a^i \\ p_b^i \end{bmatrix} ; \quad -p_a^i = p_b^i = \left[\frac{\partial \Pi}{\partial \Delta_j}^i\right] = \left[c_j^i\right] p^i \tag{18}$$

where

$$c_j^i = \frac{L_j}{L} ; \quad p^i = \gamma_o^i e^i \tag{19}$$

c_j^i, j = 1, 2, 3, are the direction cosines and p^i is the axial force of element i in the deformed state.

By eqns(3), (4), (16), and (17), the n x (n+1) Jacobian matrix becomes

$$D\tilde{F} = [K \quad -\tilde{Q}] \tag{20}$$

where

$$K = \sum_{i=1}^{m} K_n^i ; \quad K_n^i = \left[\frac{\partial^2 \Pi^i}{\partial q_k \partial q_l}\right] \tag{21}$$

K_n^i is the tangent stiffness matrix of element i expressed relative to the generalized displacements of the assemblage. It is computed by the code number method from the global stiffness matrix of element i

$$K^i = \begin{bmatrix} \bar{K}^i & -\bar{K}^i \\ -\bar{K}^i & \bar{K}^i \end{bmatrix} \tag{22}$$

where

$$\bar{K}^i = \left[\frac{\partial^2 \Pi^i}{\partial \Delta_j \partial \Delta_k}\right] = \gamma \begin{bmatrix} \frac{L}{L_o} - (1-c_1^2) & c_1 c_2 & c_1 c_3 \\ & \frac{L}{L_o} - (1-c_2^2) & c_2 c_3 \\ \text{sym.} & & \frac{L}{L_o} - (1-c_3^2) \end{bmatrix} \tag{23}$$

$$\gamma = \frac{EA}{L} \tag{24}$$

RESULTS

To test the ability of the ODE solver to track with precision highly nonlinear equilibrium paths, the reticulated spherical cap in Fig. 2 was subjected to a variety of loads. The most revealing result was obtained by applying a load at joint 1 in the direction of the global 1-axis and tracking the equilibrium path through nine successive zero load configurations in a single run. The projections of the path onto the $\bar{\lambda}$-q_1, q_4, and q_6 planes are shown in Figs. 3-5, where the loading parameter is nondimensionalized as

$$\bar{\lambda} = \frac{\lambda 10^4}{EA} \tag{25}$$

and the joint displacements, q_k, which have units of cm, are numbered in the sequence of the global 1, 2, 3-axes from joint 1 to joint 7; i.e., q_1 and q_4 are the deflections in the direction of the global 1-axis at joints 1 and 2, respectively, and q_6 is the deflection in the global 3-axis at joint 2. The zero load configurations are labeled a-i in the sequence of occurrence, i.e., with increasing arc length. Fig. 6 shows qualitatively the positions that the elements connecting joints 1, 2, and 8 assume at the zero load states.

Figs. 2 and 6 indicate that the zero load configurations are symmetrical relative to the support plane and that a, c, g, and i

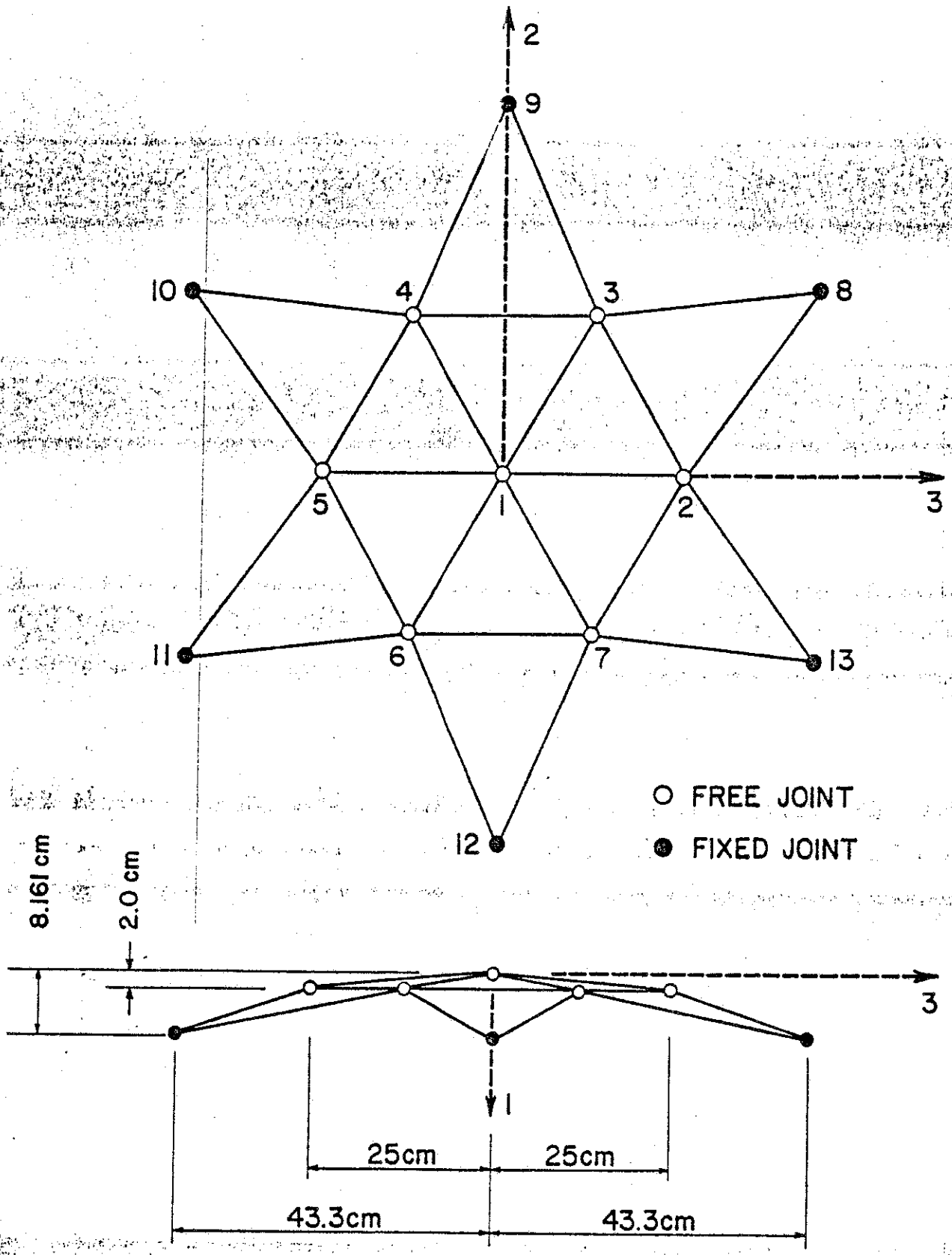
2
9
10
4
3
8
5
1
2
3
11
6
7
13
12
O FREE JOINT
FIXED JOINT
8.161 cm
2.0 cm
3
1
25cm
25cm
43.3cm
43.3cm

Fig. 2

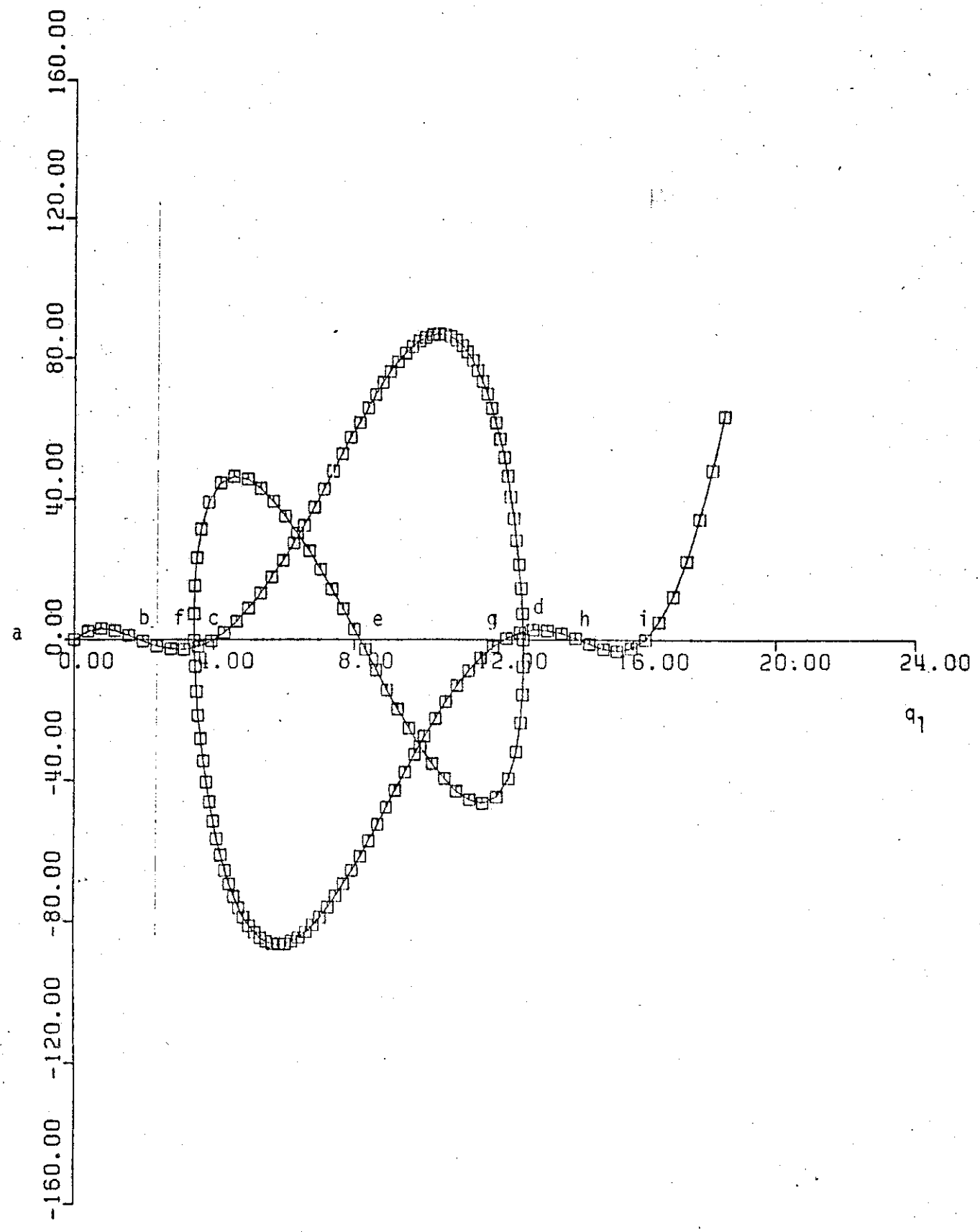
λ
160.00
120.00
80.00
40.00
0.00
-40.00
-80.00
-120.00
-160.00
a
b
f
c
e
g
d
h
i
0.00
4.00
8.00
12.00
16.00
20.00
24.00
q1

Fig. 3

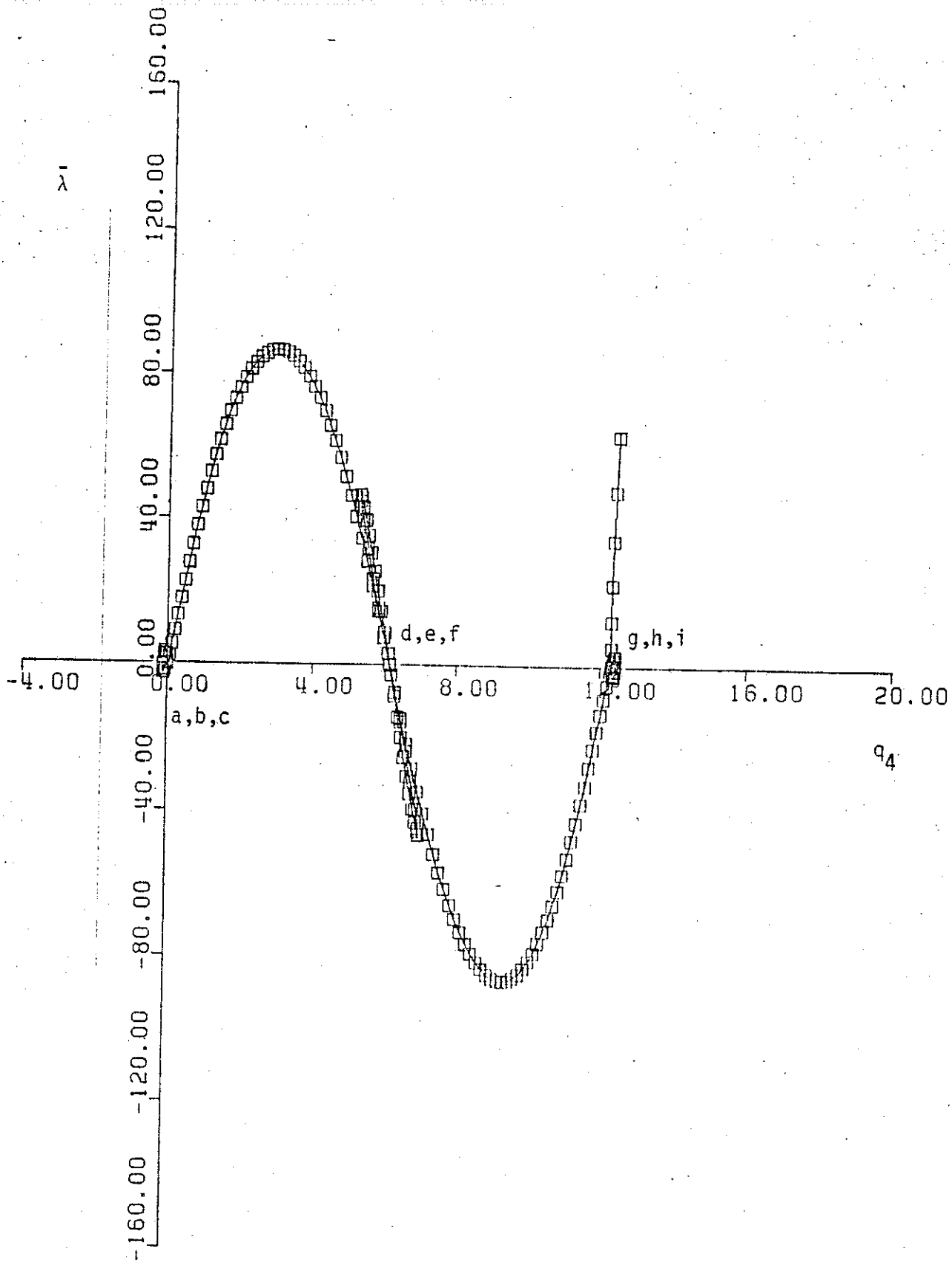
λ
160.00
120.00
80.00
40.00
0.00
-40.00
-80.00
-120.00
-160.00
-4.00
0.00
4.00
8.00
12.00
16.00
20.00
a,b,c
d,e,f
g,h,i
q_4

Fig. 4

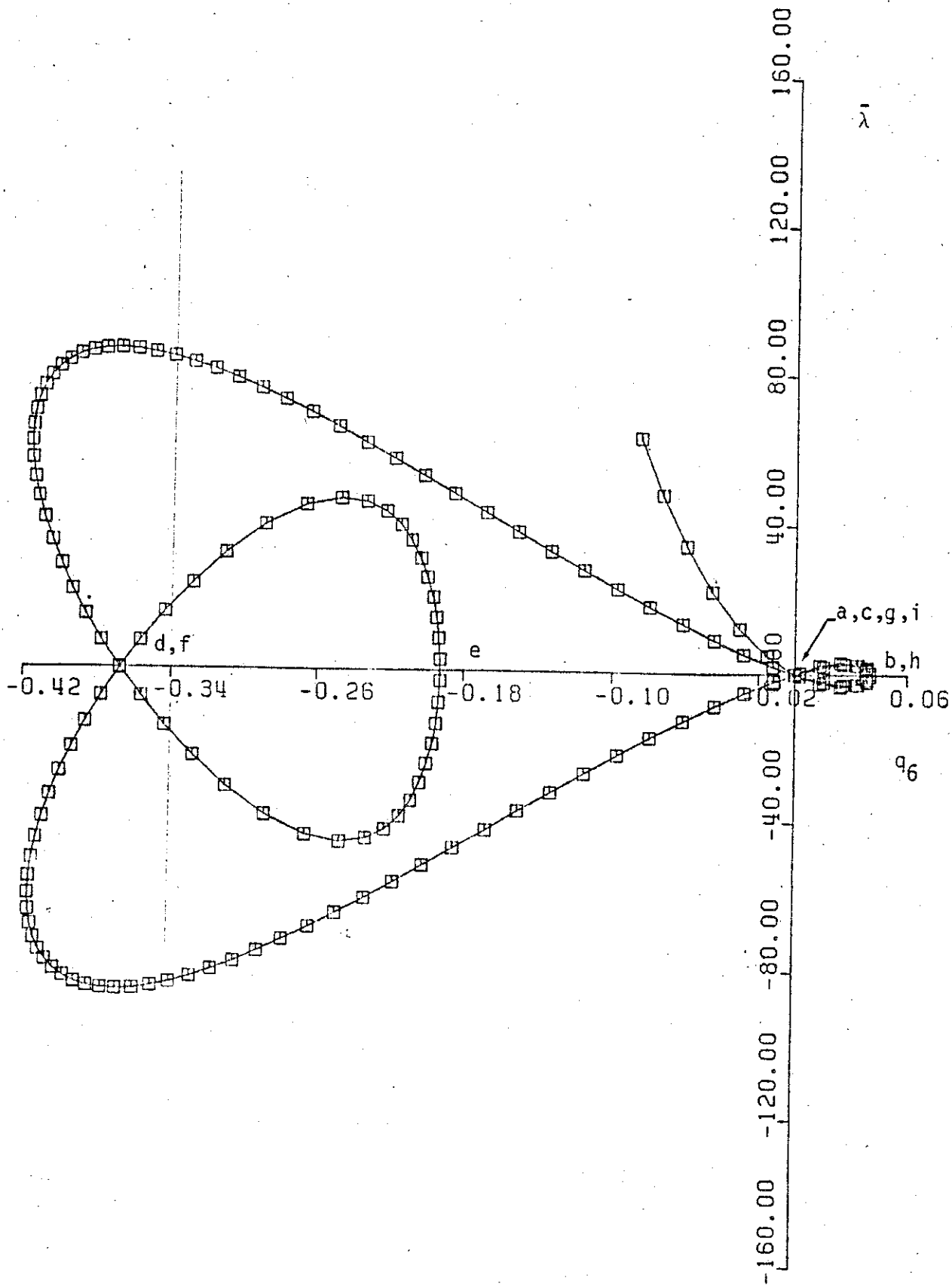
160.00
120.00
80.00
40.00
0.00
-40.00
-80.00
-120.00
-160.00
λ̄
a,c,g,i
b,h
d,f
e
-0.42
-0.34
-0.26
-0.18
-0.10
-0.02
0.06
q6

Fig. 5

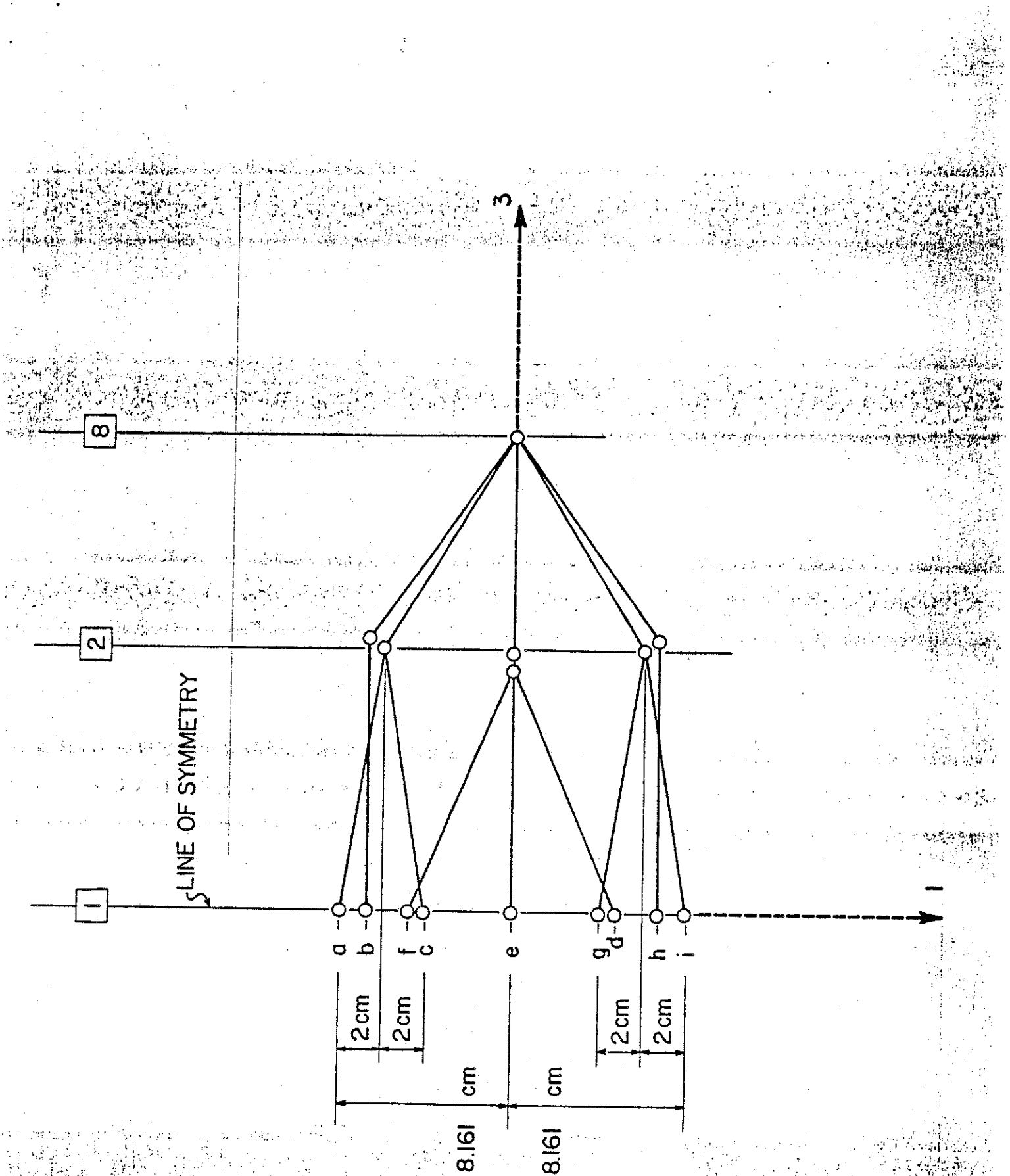
3
8
2
1
LINE OF SYMMETRY
a
b
f
c
e
g
d
h
i
2cm
2cm
2cm
2cm
8.161 cm
8.161 cm

Fig. 6

are rigid-body states. This is reflected with high precision in Fig. 5. Specifically, the curve passes twice through the largest negative coordinate on the q_6-axis, which corresponds to the zero load states d and f, and four times through the origin of the $\bar{\lambda}$-q_6 plane, which corresponds to the rigid-body states a, c, g, and i. The last pass occurs after the curve has been tracked over an arc length of approximately 60 units. This remarkable accuracy was achieved solely with the ODE solver, i.e., without a single correction by Newton's method.

The Jacobian matrix in eqn(4) has full rank along the equilibrium curve Γ for almost all $\bar{Q}$, but for some $\bar{Q}$ this may not be true, in which case Γ may bifurcate or even have an endpoint. For these special $\bar{Q}$, none of our theory is strictly applicable, and the performance of the ODE solver in the vicinity of a bifurcation point cannot be predicted. The ODE solver may go through a bifurcation point satisfactorily (i.e., points on Γ beyond the bifurcation point are computed accurately), but the branch it comes out on and the effort required to pass the bifurcation point are largely unpredictable. Precisely what happens depends on roundoff error, the ODE tolerance used, the shape of Γ, and the order and step length with which the ODE solver is operating when it reaches the bifurcation point. A successful run through a known bifurcation point, the first critical point on the fundamental equilibrium path [14], is depicted in Fig. 7. The

load distribution consists of equal loads in the direction of the global 1-axis applied at joints 2-7. q_7 represents the deflection in the direction of the global 1-axis at joint 3. The second path in Fig. 7 corresponds to a 0.1% imperfection of the load at joint 2.

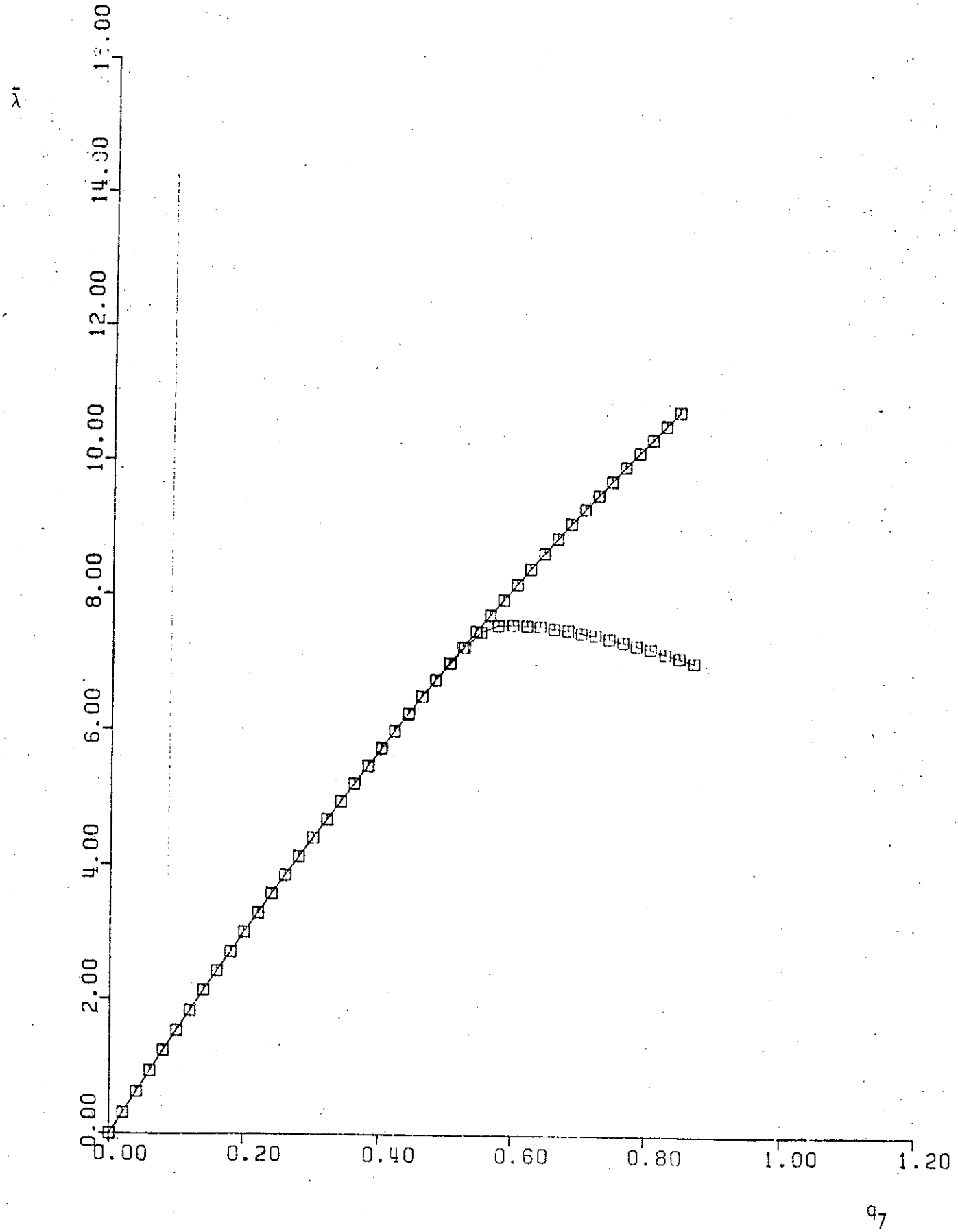
$\bar{\lambda}$
0.00
2.00
4.00
6.00
8.00
10.00
12.00
14.00
0.00
0.20
0.40
0.60
0.80
1.00
1.20
q_7

Fig. 7

REFERENCES

1. B. O. Almroth and C. A. Felippa, Structural stability. Structural Mechanics Computer Programs (Edited by W. Pilkey et al.), pp. 499-539. Univ. Press of Virginia, Charlottesville (1974).

2. L. T. Watson, A globally convergent algorithm for computing fixed points of C^2 maps, Appl. Math. Comput., 5, 297-311 (1979).

3. L. T. Watson, An algorithm that is globally convergent with probability one for a class of nonlinear two-point boundary value problems, SIAM J. Numer. Anal., 16, 394-401 (1979).

4. L. T. Watson, Fixed points of C^2 maps, J. Comput. Appl. Math., 5, 131-140 (1979).

5. L. T. Watson and D. Fenner, Chow-Yorke algorithm for fixed points or zeros of C^2 maps, ACM Trans. Math. Software, 6, 252-260 (1980).

6. L. T. Watson, Solving the nonlinear complementarity problem by a homotopy method, SIAM J. Control Optimization, 17, 36-46 (1979).

7. L. T. Watson, T. Y. Li, C. Y. Wang, Fluid dynamics of the elliptic porous slider, J. Appl. Mech., 45, 435-436 (1978).

8. C. Y. Wang and L. T. Watson, Viscous flow between rotating discs with injection on the porous disc, ZAMP, 30, 773-787 (1979).

9. L. T. Watson, Numerical study of porous channel flow in a rotating system by a homotopy method, J. Comput. Appl. Math., 7 (1981).

10. C. Y. Wang and L. T. Watson, On the large deformations of C-shaped springs, Internat. J. Mech. Sci., 22, 395-400 (1980).

11. L. T. Watson and W. H. Yang, Methods for optimal engineering design problems based on globally convergent methods, Computers & Structures, 13, 115-119 (1981).

12. W. C. Rheinboldt, Numerical analysis of continuation methods for nonlinear structural problems, Computers & Structures, 13, 103-113 (1981).

13. L. F. Shampine and M. K. Gordon, Computer Solution of Ordinary Differential Equations: The Initial Value Problem, Freeman, San Francisco (1975).

14. S. M. Holzer et al., Stability of lattice structures under combined loads. J. Engng. Mech. Div. ASCE 106 (EM2), 289-305 (1980).

15. S. M. Holzer, Static and dynamic stability of reticulated shells. International colloquium on stability of structures under static and dynamic loads, Washington, D.C., May 17-19, 1977, published by ASCE, pp. 27-39 (1977).

16. S. S. Tezcan, Simplified formulation of stiffness matrices. J. Struct. Div. ASCE 89 (ST6), 445-449 (1963).